Block generation, deformation and interaction of mass transport deposits with the seafloor: An outcrop-based study of the Carboniferous at Cerro Bola, NW Argentina.

Matheus S. Sobiesiak[1], Victoria Valdez Buso[2], Ben Kneller[2], G. Ian Alsop[2], Juan Pablo Milana[3].

[1] Programa de Pós-Graduação em Geologia, Universidade do Vale do Rio dos Sinos, 93022-000, São Leopoldo, Rio Grande do Sul, Brazil.

[2] Dept. of Geology and Petroleum Geology, University of Aberdeen, Aberdeen AB24 3UE, Scotland, U.K.

[3] Universidad Nacional de San Juan, Argentina

Corresponding author.

E-mail address: matheus.sobiesiak@gmail.com (M.S.Sobiesiak)

Abstract

Mass transport processes are notorious for their ability to carry large blocks or mega clasts, to deform sediments, and to interact with the seafloor through deformation and/or erosion of the substrate. These processes, together with their influence on slope sedimentation, are themes we address via direct field observation of three Carboniferous-aged mass transport deposits (MTDs labelled I, II and III) from Cerro Bola, NW Argentina. Internal deformation can be observed in all three MTDs, although it is best developed in MTD II, a 180 m thick vertically zoned MTD with deformation evolving upwards from a simple-shear dominated base, to a pure-shear middle zone, and finally back into a simple-shear dominated top-most zone. The contact between MTDs I and II and their underlying sandstone substrates are also locally deformed, with plastic deformation affecting up to ~20 m of substrate below the MTDs base. Conversely, the basal contact between MTD II and the substrate is also in part erosional, marked by scours and grooves that truncate the bedding in the top-most layers of the substrate. Additionally, the presence of large blocks composed of diverse lithologies embedded within the MTDs, together with the sedimentological description of the MTD´s matrix and the aforementioned interaction with the seafloor, suggest at least two processes accountable for block generation within MTDs.

Key Points

Vertical zonation of MTD II is based on soft-sediment deformation, block type and matrix behaviour.

Basal erosion and deformation is recorded below the MTDs, suggesting both frictional and plastic interaction between the MTD and the seafloor

Sandstone and siltstone blocks are present throughout the MTDs, indicating blocks may be potentially generated by at least two different processes within the same flow.

Key Words: Mass transport deposits, basal deformation, basal erosion, block generation, rafted blocks.

1 Introduction

Mass transport deposits (MTDs) are described from both seismic and outcrop data sets in terms of internal structures (e.g. Farrell 1984; Ogata *et al.* 2014; Sobiesiak *et al.* 2016b; Alsop *et al.* 2017), basal interaction (e.g. Draganits *et al.* 2008; Laberg *et al.* 2016; Sobiesiak *et al.* 2016a), creation of accommodation space (e.g. Fairweather 2015; Kneller *et al.* 2016) and presence of blocks (e.g. Macdonald *et al.* 1993; Dykstra *et al.* 2011; Alves 2015; Sobiesiak *et al.* 2016b). The internal structures of MTDs are usually described in relation to stress/strain fields, with compressional fields associated with thrust planes, reverse faults, slump folds and shear planes (e.g. Farrell 1984; Alsop *et al.* 2017; Sobiesiak *et al.* 2017), while extensional strains are expressed as normal faults, boudinage, mullions, and pull-aparts among others (e.g. Dykstra *et al.* 2011; Alsop & Marco 2014; Alves 2015).

When a MTD moves downslope, it translates over a detachment surface termed a basal shear surface (BSS) or basal glide plane. This surface is developed due to progressive shear failure and defines the lower limit of the MTD, thus separating deformed sediment above from undeformed strata below (e.g. Hampton *et al.* 1996; Frey-Martínez *et al.* 2006; Bull *et al.* 2009; Omosanya & Alves 2013). The interaction between the BSS and the substrate has been widely documented from both seismic data (e.g. McGilvery & Cook 2003; Gee *et al.* 2005; Moscardelli *et al.* 2006; Posamentier & Martinsen 2011; Alves *et al.* 2014), and more rarely from outcrop (e.g. Gawthorpe & Clemmey 1985; Lucente & Pini 2003; Butler & Tavarnelli 2006; Dykstra *et al.* 2011; Ogata *et al.* 2012; Dakin *et al.* 2013; Sobiesiak *et al.* 2016b). The nature of these interactions are usually described as erosional, creating features such as scours (Nissen *et al.* 1999; Posamentier & Kolla 2003), grooves (Posamentier & Kolla 2003; Bull *et al.* 2009), striations (Gee *et al.* 2005; Bull *et al.* 2009), and monkey fingers (McGilvery & Cook 2003). However, new studies have revealed that the interaction between an MTD and the seafloor can be entirely deformational, resulting in the development of soft-sediment deformational structures within the upper part of sediment pile that is below the detachment surface in the case of frontally-confined MTDs (Frey-Martínez et al. 2006) or immediately beneath the seafloor in frontally-emergent MTDs (e.g. Alves & Lourenço 2010; Laberg *et al.* 2016; Sobiesiak *et al.* 2016a) and lacking sediment incorporation into the flow.

In addition, blocky MTDs are increasingly recognised as a consequence of slope failure and instability (e.g. Macdonald *et al.* 1993; Alves 2015), with blocks being defined by Alves (2015) as anything larger than boulder size (>4.1m) (Blair & McPherson 1999). From seismic data, blocks have been subdivided into rafted, remnant and outrunner blocks (e.g. Prior *et al.* 1984; Nissen *et al.* 1999; Bull *et al.* 2009). However, the above distinctions are made difficult in outcrop, due to scale and limits of exposure, among other factors. On the other hand, lithological differences between blocks and their surrounding strata are easily identified at outcrop.

The main aim of this paper is to provide a summary of published data, and a comprehensive overview of three MTDs (MTD I, MTD II and MTD III) cropping out in superbly-exposed sections at Cerro Bola in La Rioja Province, NW Argentina.

In detail, we consider the following:

1. What is the nature of the interaction between MTDs and the seafloor, and how deep can this interaction penetrate?
2. How does deformation affect the MTD sediments themselves, and how is it distributed throughout the deposit?
3. What types of blocks occur within the MTDs, what do they represent, and what processes are capable of creating them?

2 Geological Setting

Paganzo is an epicratonic basin, resulting from the accretion of three crustal blocks (Famatina, Cuyania and Chilenia) along the western margin of the Gondwana craton, between the Ordovician and Early Carboniferous (Limarino *et al.* 2002, 2006; Desjardins *et al.* 2009). The basin is located in north-western Argentina (**Fig.01**) extending over an area of 30,000km^2, and containing up to ~ 4500 metres of sediments (Paganzo Group) (Ramos 1988). The basin is bound to the north by the Alto de La Puna, to the south and east by the Pampean and Pie de Palo highs (Limarino & Spalletti 2006). To the west, the basin is limited by the Precordillera, separating Paganzo from the western basins of Calingasta-Uspallata and Rio Blanco.

Fernandez-Seveso & Tankard (1995) and Azcuy *et al.* (1999) subdivided the Paganzo Group into three Formations: Guandacol, Tupe and Patquia. The Guandacol Formation was affected by the Late Paleozoic glaciation, and records at least three glacial/deglacial cycles, resulting in a glacially-derived package overlain by thick proglacial and postglacial marine packages, including deltaic sediments, black shales, turbidites and mass transport deposits suggesting a periglacial environment) (Fernandez-Seveso & Tankard 1995; Limarino *et al.* 2002; Milana *et al.* 2010; Valdez Buso 2015). The Tupe Formation is characterised by sediments deposited in fluvial, lacustrine and marginal marine environments, and the Pataquia Formation consists of a red bed succession comprising alluvial fan, fluvial and playa lake lithofacies encroaching on a marginal to shallow marine environment.

Cerro Bola is a mountain located at the border between La Rioja and San Juan Provinces, near the town of Villa Union (~30 km SW) (**Fig.01 and 02**). Structurally, the mountain consists of a large north–south trending, west-vergent periclinal anticline that forms the hanging-wall to a thrust system that dips eastward at ~24° (Milana *et al.* 2010).The thrust system is related to the Neogene to Quaternary Pampean Range orogenic deformation (Zapata & Allmendinger 1996) The sedimentary succession at Cerro Bola was deposited on the western margin of Paganzo Basin, exposing Carboniferous sediments from the Guandacol Fm to Permian red beds of the Patquia (Milana *et al.* 2010). The Guandacol Fm is related to glaciogenic lithostratigraphy (Valdez *et al.* 2015), and in the Cerro Bola area the relation of this formation with Tupe- and Pataquia Fm is to date still poorly understood (Valdez *et al.* 2015). At least three major glacial / deglacial cycles are recorded in Cerro Bola (e.g. Milana *et al.* 2010; Dykstra *et al.* 2011; Valdez *et al.* 2015; Fallgatter *et al.* 2016).

The Guandacol stratigraphy preserved at Cerro Bola encompasses roughly ten units that can be traced confidently across the mountain side (from base to top): a Fluvio-Deltaic sequence (FD I); an MTD (MTD I) that contains sandstone blocks; another Fluvio-Deltaic unit (FD II) displaying an eroded top; an MTD (MTD II) that also contains sandstone blocks; ponded turbidite sandstones; black shales (maximum flooding zone); turbidite sandstones package; Fluvio-Deltaic sequence (FD III); an MTD (MTD III); a Fluvio-Deltaic sequence (FD IV) and then everything is capped by Permian red beds (Pataquia Fm) (Milana *et al.* 2010) (**Fig.01 and 02**). In total the stratigraphic thickness cropping out in Cerro Bola exceeds 1 km (Milana *et al.* 2010; Dykstra *et al.* 2011) (**Fig. 01 and 02**).

3 Mass transport deposits at Cerro Bola

Cerro Bola is a strike section through part of the Paganzo Basin, with a ~ 1200 metres thick stratigraphic succession exposed at outcrop that extends for 10 kilometres in length with excellent two and three-dimensional exposure (**Fig. 02**). At Cerro Bola we describe three MTDs exposed along the mountain side, the first two MTDs (MTD I and MTD II) are the most accessible, and both possess outsized sandstone and siltstone blocks, internal deformational structures as well as signs of interaction with the underlying substrate (Dykstra *et al.* 2011; Valdez *et al.* 2015; Fallgatter *et al.* 2016; Sobiesiak *et al.* 2016b). The third, MTD III, differs from the older two, and displays a deeply incised basal surface that cuts into the upper surface of the underlying sandstone deposit (Milana *et al.* 2010; Valdez *et al.* 2015).

3.1 MTD I

MTD I is the oldest exposed at Cerro Bola, and only outcrops in the core of the anticline (**Fig. 02 and 03a**). The deposit, which is ~115 metres thick and outcrops for ~1.5 kilometres along depositional strike, consists of a massive green-coloured silty matrix (**Fig. 03a and b**) with pebbles, cobbles and boulders of coarse-grained granitoid and metamorphic rocks originating from the Precambrian basement (Valdez *et al.* 2015). The MTD contains blocks of sandstone (**Fig. 03b**) that range in size from ~3 to 5 metres in diameter. These light orange sandstone blocks are composed of massive medium- to coarse-grained sandstone. Additionally, blocks of green-coloured, undeformed to moderately deformed bedded siltstone can be found throughout the MTD (**Fig. 03c**). The deposit matrix possesses no real markers, making internal soft-sediment deformation difficult to recognize (Valdez *et al.* 2015).

However, we do record a ~14 m thick zone showing intense ductile deformation in the upper zone of the Fluvio-Deltaic sediments (FDI) directly below MTD I (**Fig. 03d**), which we infer to have occurred while the sediment was unlithified. The deformation includes highly-deformed sediments that contain pinch and swell structures, along with various scales of folding and sheared matrix. According to Valdez *et al.(*2015), the deformation style resembles ductile structures described in metamorphic rocks. The majority of sandstone blocks within MTD I occur near the base.

Valdez *et al.(*2015) described MTD I from Cerro Bola and Sierra de Maz, a locality ~10 kilometres northwest of Cerro Bola that exposes the same glacially-influenced stratigraphy. Here, they were able to identify a 20 metre thick turbidite package composed of dark brown, medium- to coarse grained sandstone capped by black shale deposited atop MTD I. These turbidites are locally developed in Sierra de Maz and are interpreted as deposits restricted by MTD topography, termed ponded turbidites. Equivalent ponded turbidites are not found above MTD I in Cerro Bola.

3.1.1 Interpretation

MTD I is interpreted to be produced from the failure of accumulations of ice rafted debris, or ‘aquatill’, where basement clasts contained within the matrix are interpreted to be remobilized drop-stones. Stratified siltstone blocks are considered to be coherent remnants of the original sediments that were more rigid and survived the flow deformation. This interpretation is based on the similarities between the average composition of the siltstone blocks and the MTD matrix. The sandstone blocks may originate from the erosion of the substrate, or from sandstones within a heterogeneous MTD protolith. It is impossible to distinguish between these alternative models due to the lack of directly supporting data (for example, evidence for basal erosion) and the sandstone blocks may in fact originate from a combination of both substrate erosion and disintegration of a heterogeneous protolith.

The flow is considered to be dominated by pure shear deformation, due to the boudinage of sandstone and siltstone blocks. Regardless of whether the MTD as a whole is dominated by pure shear, there must have been a significant component of simple shear operating at least along the lower boundary, as shown by the ~14 metre thick deformational zone recorded at the contact between the MTD and the sandy substrate. Valdez *et al.* (2015) suggest that sandstone blocks may owe their origin to substrate deformation and shearing, followed by their consequent incorporation into the translating flow.

3.2 MTD II

MTD II is up to ~180 metres thick and crops out for over ~8 kilometres along strike (Milana *et al.* 2010; Dykstra *et al.* 2011; Sobiesiak *et al.* 2016a, b) (**Fig. 02**). Moreover, it is the most accessible, best exposed and therefore the most studied of Cerro Bola’s MTDs.

In general, MTD II is very similar to MTD I, consisting of green, fine-grained, silty sediments that are remobilized and highly-sheared (**Fig. 04a**). The matrix contains granule to boulder-size clasts of Precambrian granitoid and metamorphic basement rocks, sandstone and siltstone blocks (**Fig. 04a**), and ball-shaped concretions (which give the name “Bola” to the mountain). MTD II has irregular boundaries, with the upper boundary displaying onlap of overlying sediments, together with local slumping away from regions of higher surface topography (e.g. Fairweather 2015; Kneller *et al.* 2016) (**Fig. 04b**). The lower boundary is marked by two styles of basal interaction. The first consists of basal scours that cut into and ‘pluck’ parts of the underlying Fluvio-Deltaic sandstone (Dykstra *et al.* 2011; Sobiesiak *et al.* 2016b) (**Fig. 02 and 04a**). The second type of basal interaction is where ductile shear of unlithified sediment is developed directly below the base of the MTD (Sobiesiak *et al.* 2016a) (**Fig. 04c**). Additionally, MTD II is vertically zoned and can be stratigraphically divided into three distinct lower, middle and upper units with transitional boundaries, according to variations in texture and structures (Dykstra *et al.* 2011; Sobiesiak *et al.* 2016b) (**Fig. 04a**).

Sandstone and siltstone blocks are present throughout the whole of MTD II. In general, whitish to orange sandstone blocks comprise medium- to coarse-grained, moderately sorted arkosic sandstone (**Fig. 04a, d and e**). The blocks are highly fractured, generally with no discernible internal structure, but locally primary features such as large-scale trough cross-stratification, ripples and climbing ripples are recorded (Garyfalou 2015; Sobiesiak *et al.* 2016b) (**Fig. 04d and e**). Usually, the margins of sandstone blocks display interaction with the MTD, marked by the shearing and/or deformation of the surrounding matrix (Milana *et al.* 2010; Dykstra *et al.* 2011; Sobiesiak *et al.* 2016b). Light to dark green siltstone blocks (Dykstra *et al.* 2011) are composed of sandstone, siltstone and dark mudstone layers, with each layer ranging in thickness from millimetres up to 10 centimetres (Sobiesiak *et al.* 2016b). Random granule to boulder sized clasts are preserved within siltstone blocks, where the layers below and above are deflected around these clasts. Siltstone blocks display only weak internal ductile deformation, but are highly fractured. A full description of sandstone and siltstone blocks from MTD II can be found in Sobiesiak *et al.* (2016b).

The lower zone of MTD II ranges from 40 up to 60 metres in thickness (Sobiesiak *et al.* 2016b), and is characterised by the occurrence of sandstone blocks within a variably sand-rich matrix and sand streak lithology. Sandstone blocks locally comprise ~30% of the MTD exposure ranging from a few metres up to ~90 m long and up to ~15m thick (Sobiesiak *et al.* 2016b) (**Fig. 04a**). Additionally, there is a vertical distribution of blocks, with larger and more irregular blocks found near the base of MTD II (Sobiesiak *et al.* 2016a). Sand streak lithology is similar to the sandstone blocks and the underlying substrate (Garyfalou 2015), with sand streaks being very abundant near sandstone blocks, and close to the contact with the substrate. Sand streaks record complex deformation with superimposed strain histories (Dykstra *et al.* 2011; Sobiesiak *et al.* 2016b). The sand-rich matrix is present throughout the whole lower zone of MTD II, although the amount of sand entrained within the matrix decreases vertically through the deposit.

The contact between the lower and middle zones of MTD II is transitional over ~15 m, and marked by the vertical decrease and eventual disappearance of sand entrained into the silty matrix (Sobiesiak *et al.* 2016b). The middle zone is itself characterised by the presence of siltstone blocks within a silty matrix, and ranges in thickness from 50 up to 90 metres (Sobiesiak *et al.* 2016b). The matrix to the middle zone is composed of highly sheared and fractured green siltstone, containing granitoid and metamorphic clasts. Sandstone blocks are still present, but are less frequent and generally smaller when compared with those in the lower zone. Large-scale folding and boudinage of sandstone blocks is observed in the middle zone.

The contact between the middle and the upper zone of MTD II is transitional, and is marked by the presence of a thick, folded and fractured turbidite sandstone bed including a metre-thick mud cap (megabed), intermittently distributed along the lower portion of the upper zone. The upper zone is 40 to 60 metres thick (Sobiesiak et al. 2016b), with the green siltstone matrix containing basement clasts. Sandstone and siltstone blocks are less frequent and much smaller than those from the underlying zones. The upper zone is marked by the occurrence of thrust zones, large-scale folding and thrust fault imbrication (Dykstra *et al.* 2011; Sobiesiak *et al.* 2016b).

Soft-sediment deformation can be found throughout the whole of MTD II, with folds and faults being the most commonly observed structures. The lower zone contains the greatest concentration of structures, although this might simply reflect the presence of distinct sandy markers within the matrix that readily record and highlight the deformation. Other structures such as, mullions, boudins, shear lozenge, pull-aparts, sheath folds, bookshelf (dominoes) faulting, and flame structures are observed throughout the MTD (Sobiesiak *et al.* 2016b).

The lower boundary of MTD II is extremely irregular where erosional features cut into the underlying sandstone to create scours, gouges and/or grooves (Dykstra *et al.* 2011; Sobiesiak *et al.* 2016b) (**Fig. 02**). These erosional depressions range in size from couple of metres up to ~100s metres in length and up to ~20 metres deep (Sobiesiak *et al.* 2016b). Additionally, soft-sediment deformation affects the uppermost ~20 metres of the underlying sandstone sequence (Milana *et al.* 2010; Sobiesiak *et al.* 2016a) (**Fig. 04c**). Deformation of the substrate starts at the contact with MTD II, and continues downwards until a sharp shear surface defines the boundary between the deformed and undeformed substrate. Deformation of the substrate is recorded in a series of soft-sediment structures such as recumbent, overturned, parasitic (S and Z) fold types, boulder rotation, boudins, pinch and swell structures, mullion structures, bed attenuation and the formation of proto-block shaped structures.

The upper boundary of MTD II is recorded by a succession of turbidites that show interaction with the topographic top surface of the MTD at different scales (Fairweather 2015; Kneller *et al.* 2016) (**Fig. 04a and b**). The turbidites vary from 0 to ~60 metres thick, and have been subdivided into five stratigraphic units according to their style of topographic filling (Fairweather 2015). In general they consist of massive to rippled and normally graded beds of coarse to fine-grained light yellow sandstone that are capped by siltstone and mudstone. Sitting directly on top of the MTD is a single, green turbidite that drapes the topography and is interpreted as being cogenetic to MTD II (Dykstra *et al.* 2011; Kneller *et al.* 2016; Sobiesiak *et al.* 2016b; Fallgatter *et al.* 2017) (**Fig. 04b**). The first units occur as isolated lenses that onlap topographic highs on the upper surface of MTD II and locally slump off it. The topographic irregularities are interpreted as isolated basins that are progressively filled and buried over time, first those at a small scale (few metres in amplitude, and metres in wavelength), into intermediate (10s of metres in amplitude, 500-1000 metres in wavelength) and finally into large length scales (6500 metres, with amplitudes of the order of 100 metres), which affect only the upper and more extensive units (Fairweather 2015; Kneller *et al.* 2016).

3.2.1 Interpretation

MTD II has similar characteristics to MTD I, such as the presence of sandstone and siltstone blocks, basal deformation, basement clasts and greenish silty matrix. Consequently MTD II is interpreted to be the result of glacially-influenced sediments (ice-rafted debris) having undergone remobilization. Crystalline clasts embedded in the matrix are interpreted as drop-stones, siltstone blocks as the least deformed end-member of the MTD protolith (Dykstra *et al.* 2011; Sobiesiak *et al.* 2016b) and sandstone blocks as derived from seafloor erosion. The interpretation of seafloor erosion and subsequent incorporation of sandstone blocks into MTD II is supported by field observations such as; erosional surfaces cutting into the underlying sandstone; petrographic resemblance between sandstone blocks and substrate sandstone (Garyfalou 2015); and even a block apparently arrested in the process of entrainment into the MTD (Sobiesiak *et al.* 2016a, b). The broad zonation of MTD II is interpreted to be due to different deformational styles affecting each of the zones. The lower zone is considered to be dominated by simple shear, leading to sand streaks, while the middle zone comprises a greater component of pure shear leading to boudinage. The upper zone is associated with simple shear deformation resulting in fold and thrust systems. Additionally, the ~20 m thick zone of deformation below MTD II is interpreted to reflect shear of underlying sediments created as the MTD moved downslope. When grouped together with erosional scours, this indicates a complex morphology and behaviour of the basal shear surface, as well as variations in flow and substrate properties. Turbidites deposited on top of MTD II are interpreted as ponded turbidites, as they markedly onlap the topographic relief created during MTD movement (Dykstra *et al.* 2011; Valdez *et al.* 2015; Sobiesiak *et al.* 2016a, b).

3.3 MTD III

MTD III is up to ~120 metres thick and crops out for ~10 kilometres along depositional strike. It is the most difficult of the Cerro Bola MTD’s to access due to its high stratigraphic position on the mountain. In general the MTD consists dominantly of a dark green coloured siltstone, that can be broadly subdivided into two zones (lower and upper) according to its internal deformation and stratification (**Fig. 05a, b and c**). At the northern and southern areas of Cerro Bola, the lower zone comprises about ~50 metres of the deposit and displays coherently bedded sediments (**Fig. 05a, b and c**), only locally deformed (Valdez *et al.* 2015). It consists of thin (~ 10s of cm thick) sand beds with abundant rippled surfaces and convolute bedding, including clasts (drop-stones) with deflected layers above and below, interbedded with mudstone and more rarely shales. The upper zone of the deposit is extensively deformed, composed of folded and/or disrupted sandstone beds in a silty rich matrix. Additionally, scattered pebbles, cobbles and boulders of crystalline basement rocks are also present. In the central part of the inlier, however, the whole of MTD III (lower and upper zone) is deformed and displays soft-sediment deformation features such as slump folds (Valdez *et al.* 2015).

The base of MTD III is marked by the occurrence of an E-W trending erosional surface (**Fig. 05a, b**) that is clearly exposed for at least 1.5 km, and forms a truncation surface that cuts into the underlying sandstone beds (Fluvio-Deltaic 3) (Valdez *et al.* 2015). The underlying sandstones are sharply cut by this surface causing up to ~150 m of sandstones to be excised, and locally reaching almost complete removal (**Fig. 05b**). Additionally, the erosional surface locally displays a polished plane containing striations aligned towards 320^{o} – 140^{o} (Puigdomenech Negre 2014). A unit of purplish conglomeratic sandstones that are irregularly distributed in lenticular bodies appear to lie within incisions into this surface. The incised sandstones are stratified and towards the top of the sequence display traction features, such as cross bedding (Valdez *et al.* 2015). The upper boundary of the deposit locally display a succession of turbidite beds that pinch out laterally (**Fig. 05d**) and onlap against the MTD top.

3.3.1 Interpretation

MTD III consists largely of ice-rafted debris, together with possible turbidite, much of which has been remobilized and transported downslope as a MTD. The erosion surface might be interpreted as the slide scar of a mass movement (Valdez *et al.* 2015). Alternatively, the erosional surface locally displays a U shaped morphology (see figure 10b in Valdez et al.2015) which taken together with the polished striated surfaces described by Puigdomenech Negre (2014) could be interpreted as the product of glacial movement. Finally, the surface may represent an incised valley in the top of the delta. The lower zone of MTD III, where it is coherently bedded and relatively undeformed, may represent large coherent slide blocks or MTD protolith still in its original position. Lastly, the turbidites deposited on top of the MTD are interpreted as ponded turbidites, denoting confinement by the interaction of these flows with the rugged MTD topographic surface.

4 Discussion

4.1 Seafloor interaction

Studies of the interaction of MTDs with the seafloor have recently been undertaken using both outcrop and seismic data (e.g. Prior *et al.* 1984; Gee *et al.* 2005; Moscardelli *et al.* 2006; Alves & Lourenço 2010; Laberg *et al.* 2016; Sobiesiak *et al.* 2016a). The documented interaction is considered to occur in two styles, erosional and deformational, which are not mutually exclusive. The erosional power of MTDs at Cerro Bola can be recognized from MTD II and III, with the former displaying basal irregularities interpreted as scours and/or grooves cutting down into the underlying sandstone (**Fig. 02**), while the latter displays a ~150 metres incision into substrate (**Fig. 05a and b**). Additionally, MTD I and II both contain sandstone blocks (**Fig. 03b, 04a, d and e**), which are similar in composition to the underlying sandstones, and may be interpreted as being derived from erosion of the substrate (Garyfalou 2015; Sobiesiak *et al.* 2016b).

Laberg *et al.* (2016) described an MTD from the Nankai Trough, SE Japan, where five sudden indentations were recorded in the basal shear surface. However, this MTD had no seismic-scale blocks, and the indentations were interpreted as slabs detached at different stratigraphic levels during slope failure. Alternatively, Gee *et al.(*2005) documented linear features scoured in the seafloor, which the authors interpreted as grooves. The process of groove-making is described as the dragging of a tool (such as rigid blocks) contained at the base of the flow that would scour the substrate. This would mean that seafloor erosion could also be a consequence of blocks. Moscardelli *et al.* (2006) also described erosional features from offshore Trinidad, where the main reason for seafloor scouring was due to the erosive power of the flow that transitioned from a confined into a partially confined setting. In summary, a range of factors may influence sea floor erosion, ranging from the presence of large blocks that may create grooves, weak layers within the seafloor sediments, to variations in flow dynamics that lead to wider erosive features.

The other type of MTD interaction relates to deformation of the sea floor. This is well illustrated at Cerro Bola by MTD I and II, which respectively display a ~14 m (**Fig. 03d**) and a ~20 m thick (**Fig. 04c**) deformation zone localized in the uppermost layers of the substrate sandstone. Penetration of the strain profile into the substrate resulted in the development of soft-sediment deformation (folds, boudins, proto-blocks, among others) spread throughout the whole affected area. The lower contact of the deformed substrate is bounded by a sharp shear zone that clearly separates deformed from undeformed and evenly bedded sediments. Such basal deformation has been described by only a few authors from outcrop (Alves & Lourenço 2010; Butler & McCaffrey 2010; Valdez *et al.* 2015; Sobiesiak *et al.* 2016a), core (Laberg *et al.* 2016) and more rarely from seismic data (Alves 2015). We suggest that the stress exerted by the flow is not restricted to its base, but penetrates a considerable distance into the substrate, thus deforming it. Similar observations were made by Alves & Lourenço

(2010) and Laberg *et al.* (2016) where the basal shear zone lay within and deformed the sandy substrate.

Additionally, the depth of penetration of deformation into the substrate in relation to the height of the overlying MTD was calculated, using both Carboniferous MTD I and II from Cerro Bola and, as a comparison, a Neogene MTD from SE Crete described by Alves & Lourenço (2010). From Cerro Bola the deformation zone of MTD II was ~11% of the total thickness of the overlying MTD; and for MTD I it was ~12%; while Alves & Lourenço (2010) calculated the deformation as ~15% of the total thickness of the overlying MTD. The observations above support the conclusion that in some cases the basal shear surface of an MTD can be considered as a zone rather than a discrete surface (Alves & Lourenço 2010). Unfortunately, the variables that control the formation of these zones are at present poorly known, although it could be conjectured that the significant factors will likely be those that control the shear stress of the MTD (mainly the speed of movement, thickness and density) and, the yield strength and rheology of the substrate (controlled by degree of lithification, fluid pressure and lithologies).

4.2 Towards a model for block generation

Blocks within MTDs are frequently classified into rafted, remnant and outrunner blocks (e.g. Prior *et al.* 1984; Bull *et al.* 2009; Posamentier & Martinsen 2011; Alves 2015). Outrunners are defined as those blocks that are detached from the leading edge of the MTD and have moved downslope beyond the front of the flow (e.g. Prior *et al.* 1984; Bull *et al.* 2009). They are associated with a type of basal erosion called glide-tracks and the blocks themselves are not found embedded within the MTD, but at the end of the glide-track (Prior *et al.* 1984; Nissen *et al.* 1999). Remnant blocks are defined as “isolated blocks of material that have not experienced failure” (Bull *et al.* 2009). These blocks are bounded by sets of faults and are vertically connected with underlying non-MTD substrate, thus lacking basal disruption (Alves & Cartwright 2009; Alves 2015). Rafted blocks, on the other hand, behave as a ‘coherent block’ transported downslope by the flow, and are usually described as "floating within the disaggregated chaotic matrix of the MTD" (Alves 2015). Rafted blocks are also called 'translated' or 'intact' blocks (e.g. Masson *et al.* 1993; Bull *et al.* 2009). All blocks described from Cerro Bola are classified as rafted blocks.

Analysis of MTD I and II from Cerro Bola, provides an opportunity to differentiate rafted blocks into sandstone and siltstone blocks, according to their lithological differences, and classify them into either "native" (intra-formational) or "exotic" (extra-formational) in respect to their genetic relation to the host and/or encasing lithology (e.g. Masson *et al.* 1993; Haughton *et al.* 2003; Lucente & Pini 2003; Jackson *et al.* 2009; Ogata *et al.* 2014b; Festa *et al.* 2016). The sandstone blocks in general are composed of a whitish to orange sandstone and appear to be derived by erosion of the substrate (**Fig. 04d and e**). These sandstone blocks are interpreted as exotic blocks, and are thus considered to be coherent fragments of externally-sourced material of different lithology from the MTD, and potentially displaying distinct rheological behaviour from the flow matrix. MTD II shows clear interaction with the underlying sandstone deposit in the form of irregular gouges and /or grooves (described above). Additionally, in places, it is possible to see blocks arrested in the process of entrainment by the flow. Such evidence corroborates the interpretation that the blocks originated from the shearing of the underlying unit. A notable observation is that blocks can originate by substrate erosion. However, at the same time, the presence of blocks can produce seafloor erosion through the process of groove-making or tooling.

Within MTD II block size and frequency diminishes upwards through the deposit (**Fig. 04a**). To explain this vertical distribution, a model was proposed by Sobiesiak *et al.* (2016a) in which large sandstone blocks ascended through the MTD matrix via buoyancy. First, the blocks of varying sizes would be eroded from the underlying substrate and incorporated into the base of the flow. The blocks would rise through the matrix by virtue of their lower density. As they ascend they would undergo shear-stripping, stretching and/or fragmentation, depending on the behaviour of the matrix and the contrast in material properties between block and matrix. This process would reduce the size of blocks as they move up, resulting in smaller blocks higher in comparison with those at the base. Additionally, the accumulation of blocks at the base of the flow can be explained by other factors; (i) it is the closest part of the MTD to their point of origin; and/or (ii) some blocks possess neutral-buoyancy, or may be even denser than the matrix, therefore fostering the accumulation of blocks along the basal contact.

Siltstone blocks, on the other hand, are interpreted as native blocks, comprising light to dark green layered siltstone (**Fig. 03c**) and are considered to be the least-deformed remnants of the MTD protolith (Dykstra *et al.* 2011; Valdez *et al.* 2015; Sobiesiak *et al.* 2016b). The siltstone blocks are interpreted as being derived from the same source material or lithology as the main MTD body. The rheological behaviour of siltstone blocks does not differ significantly from the overall flow, and they are more or less evenly distributed throughout the MTDs stratigraphy (Sobiesiak *et al.* 2016b). However, there are places where siltstone blocks are difficult to distinguish from the actual MTD matrix due to their similarity with the matrix, and the indistinct bedding that can be confused with matrix fractures. In conclusion, siltstone blocks are interpreted as remnants of the MTD protolith, and because they have a similar rheology and density to the MTD matrix, would simply be carried passively downslope by the moving flow. Such rafts would get progressively smaller due to their fragmentation during transport, as shown by Alves & Cartwright (2009). Nevertheless, care must be taken when classifying blocks; on some occasions MTDs may have a heterogeneous origin including a range of lithologies, and the resulting blocks may display a different lithology from the desegregated, mixed and homogeneous host matrix.

5 Conclusions

We have summarized and discussed the main aspects and structures of three Carboniferous MTDs exposed at Cerro Bola. The main conclusions can be summarized as follows:

(i) Two types of basal interaction are developed that demonstrate the erosional and/or deformational power of MTDs. Seafloor deformation is recorded below

MTD I and II and erosion is recorded below MTD II and III. The character and nature of the interaction between the MTD and the seafloor is complex and poorly understood, though variables that influence MTD´s shear stress and the substrate rheology and yield strength are significant factors that would influence the occurrence, style and thickness of erosion and/or deformation zone.

(ii) MTD rafted blocks can be generated by two means. First, by the disaggregation of the MTD protolith, imparting similar properties to the block as the main MTD body. Therefore, such blocks are more likely to preserve original features or undergo less deformation as they may only ‘float’ within the matrix. Second, by the erosion of the seafloor, where the blocks are made of externally sourced material and of different lithology with respect to the MTD matrix, potentially exhibiting mechanical behaviour distinctly different from the overall flow. Consequently, these blocks may be reworked by the flow due their contrast in physical properties.

(iii) Additionally, the presence of “exotic” blocks within the MTD is not strictly indicative of erosion, since MTDs can have a heterogeneous source composed of multiple lithologies. Also exotic blocks can be the result of seafloor erosion and/or can tool the seafloor and be the agent of erosion.

Acknowledgments

The research presented here was carried out with support from CNPq-Brazil (National Council for Scientific and Technological Development) in partnership with Shell-Brazil. We thank Massimo Moretti and an anonymous reviewer, whose constructive comments and criticisms helped to improve the text, their efforts are highly appreciated. Finally, we thank Kei Ogata, Gian Andrea Pini and Andrea Festa for editing this volume.

References

Alsop, G.I. & Marco, S. 2014. Fold and fabric relationships in temporally and spatially evolving slump systems: A multi-cell flow model. *Journal of Structural Geology*, **63**, 27–49, https://doi.org/10.1016/j.jsg.2014.02.007.

Alsop, G.I., Marco, S., Levi, T. & Weinberger, R. 2017. Fold and thrust systems in Mass Transport Deposits. *Journal of Structural Geology*, **94**, 98–115, https://doi.org/10.1016/j.jsg.2016.11.008.

Alves, T.M. 2015. Submarine slide blocks and associated soft-sediment deformation in deep-water basins: A review. *Marine and Petroleum Geology*, **67**, 262–285, https://doi.org/10.1016/j.marpetgeo.2015.05.010.

Alves, T.M. & Cartwright, J.A. 2009. Volume balance of a submarine landslide in the Espírito Santo Basin, offshore Brazil: Quantifying seafloor erosion, sediment accumulation and depletion. *Earth and Planetary Science Letters*, **288**, 572–580, https://doi.org/10.1016/j.epsl.2009.10.020.

Alves, T.M. & Lourenço, S.D.N.N. 2010. Geomorphologic features related to gravitational collapse: Submarine landsliding to lateral spreading on a Late Miocene–Quaternary slope (SE Crete, eastern Mediterranean). *Geomorphology*, **123**, 13–33, https://doi.org/10.1016/j.geomorph.2010.04.030.

Alves, T.M., Strasser, M. & Moore, G.F.F. 2013. Erosional features as indicators of thrust fault activity (Nankai Trough, Japan). *Marine Geology*, **356**, 5–18, https://doi.org/10.1016/j.margeo.2013.07.011.

Azcuy, C., Carrizo, H. a. & Caminos, R. 1999. Carbonífero y Pérmico de las Sierras Pampeanas, Famatina, Precordillera, Cordillera Frontal y Bloque de San Rafael. *Instituto de Geología y Recursos Minerales Geología Argentina, Anales 29 (12): 261-318, Buenos Aires.*, **251**.

Blair, T.C. & McPherson, J.G. 1999. Grain-size and textural classification of coarse sedimentary particles. *Journal of Sedimentary Research*, **69**, 6–19, https://doi.org/10.2110/jsr.69.6.

Bull, S., Cartwright, J. & Huuse, M. 2009. A review of kinematic indicators from mass-transport complexes using 3D seismic data. *Marine and Petroleum Geology*, **26**, 1132–1151, https://doi.org/10.1016/j.marpetgeo.2008.09.011.

Butler, R.W.H. & McCaffrey, W.D. 2010. Structural evolution and sediment entrainment in mass-transport complexes: outcrop studies from Italy. *Journal of the Geological Society*, **167**, 617–631, https://doi.org/10.1144/0016-76492009-041.

Butler, R.W.H. & Tavarnelli, E. 2006. The structure and kinematics of substrate entrainment into high-concentration sandy turbidites: a field example from the Gorgoglione ‘flysch’ of southern Italy. *Sedimentology*, **53**, 655–670, https://doi.org/10.1111/j.1365-3091.2006.00789.x.

Dakin, N., Pickering, K.T., Mohrig, D. & Bayliss, N.J. 2013. Channel-like features created by erosive submarine debris flows: Field evidence from the Middle Eocene Ainsa Basin, Spanish Pyrenees. *Marine and Petroleum Geology*, **41**, 62–71, https://doi.org/10.1016/j.marpetgeo.2012.07.007.

Desjardins, P.R., Buatois, L. a., Limarino, C.O. & Cisterna, G. a. 2009. Latest Carboniferous–earliest Permian transgressive deposits in the Paganzo Basin of western Argentina: Lithofacies and sequence stratigraphy of a coastal-plain to bay succession. *Journal of South American Earth Sciences*, **28**, 40–53, https://doi.org/10.1016/j.jsames.2008.10.003.

Draganits, E., Schlaf, J., Grasemann, B. & Argles, T. 2008. Giant submarine landslide grooves in the Neoproterozoic/Lower Cambrian Phe Formation, northwest Himalaya: Mechanisms of formation and palaeogeographic implications. *Sedimentary Geology*, **205**, 126–141, https://doi.org/10.1016/j.sedgeo.2008.02.004.

Dykstra, M., Garyfalou, K., et al. 2011. Mass-Transport Deposits: Combining outcrop studies and seismic forward modeling to understand lithofacies distributions, deformation, and their seismic expression. *SEPM Special Publication*, **95**, 1–25.

Fairweather, L. 2015. *Mechanisms of Supra-MTD Topography Generation and the*

Interaction of Turbidity Currents with Such Deposits. Unpublished PhD thesis, University of Aberdeen.

Fallgatter, C., Kneller, B., Paim, P.S.G.G. & Milana, J.P. 2017. Transformation, partitioning and flow-deposit interactions during the run-out of megaflows Talling, P. (ed.). *Sedimentology*, **64**, 359–387, https://doi.org/10.1111/sed.12307.

Farrell, S. 1984. A dislocation model applied to slump structures, Ainsa Basin, South Central Pyrenees. *Journal of structural geology*, **73**, 727–736, https://doi.org/http://dx.doi.org/10.1016/0191-8141(84)90012-9.

Fernandez-Seveso, F. & Tankard, A.J. 1995. Tectonics and Stratigraphy of the Late Paleozoic Paganzo Basin of Western Argentina and its Regional Implications. *Petroleum Basins of South America*, 285–301.

Festa, A., Ogata, K., Pini, G.A., Dilek, Y. & Alonso, J.L. 2016. Origin and significance of olistostromes in the evolution of orogenic belts: A global synthesis. *Gondwana Research*, **39**, 180–203, https://doi.org/10.1016/j.gr.2016.08.002.

Frey-Martínez, J., Cartwright, J. & James, D. 2006. Frontally confined versus frontally emergent submarine landslides: A 3D seismic characterisation. *Marine and Petroleum Geology*, **23**, 585–604, https://doi.org/http://dx.doi.org/10.1016/j.marpetgeo.2006.04.002.

Garyfalou, K. 2015. *Integrated Analysis of Mass-Transport Deposits: Outcrop, 3D Seismic Interpretation and Fast Fourier Transform*. Unpublished PhD thesis, University of Aberdeen.

Gawthorpe, R.L. & Clemmey, H. 1985. Geometry of submarine slides in the Bowland Basin (Dinantian) and their relation to debris flows. *Journal of the Geological Society*, **142**, 555–565, https://doi.org/10.1144/gsjgs.142.3.0555.

Gee, M.J.R., Gawthorpe, R.L. & Friedmann, J.S. 2005. Giant striations at the base of a submarine landslide. *Marine Geology*, **214**, 287–294, https://doi.org/10.1016/j.margeo.2004.09.003.

Gulbranson, E.L., Montanez, I.P., Schmitz, M.D., Limarino, C.O., Isbell, J.L., Marenssi, S. a.

& Crowley, J.L. 2010. High-precision U-Pb calibration of Carboniferous glaciation and climate history, Paganzo Group, NW Argentina. *Geological Society of America Bulletin*, **122**, 1480–1498, https://doi.org/10.1130/B30025.1.

Hampton, M.A., Lee, H.J. & Locat, J. 1996. Submarine landslides. *Reviews of Geophysics*, **34**, 33–59, https://doi.org/10.1029/95RG03287.

Haughton, P.D.W., Barker, S.P. & McCaffrey, W.D. 2003. ‘Linked’ debrites in sand-rich turbidite systems - origin and significance. *Sedimentology*, **50**, 459–482, https://doi.org/10.1046/j.1365-3091.2003.00560.x.

Jackson, C.A.-L., Zakaria, A.A., Johnson, H.D., Tongkul, F. & Crevello, P.D. 2009. Sedimentology, stratigraphic occurrence and origin of linked debrites in the West Crocker Formation (Oligo-Miocene), Sabah, NW Borneo. *Marine and Petroleum Geology*, **26**, 1957–1973, https://doi.org/10.1016/j.marpetgeo.2009.02.019.

Kneller, B., Dykstra, M., Fairweather, L. & Milana, J.P. 2016. Mass-transport and slope accommodation: Implications for turbidite sandstone reservoirs. *AAPG Bulletin*, **100**, 213–235, https://doi.org/10.1306/09011514210.

Laberg, J.S., Strasser, M., Alves, T.M., Gao, S., Kawamura, K., Kopf, A. & Moore, G.F. 2016. Internal deformation of a muddy gravity flow and its interaction with the seafloor (site C0018 of IODP Expedition 333, Nankai Trough, SE Japan). *Landslides*, https://doi.org/10.1007/s10346-016-0766-7.

Limarino, C., Tripaldi, A., Marenssi, S. & Fauqué, L. 2006. Tectonic, sea-level, and climatic controls on Late Paleozoic sedimentation in the western basins of Argentina. *Journal of South American Earth Sciences*, **22**, 205–226, https://doi.org/10.1016/j.jsames.2006.09.009.

Limarino, C.O. & Spalletti, L. a. 2006. Paleogeography of the upper Paleozoic basins of southern South America: An overview. *Journal of South American Earth Sciences*, **22**, 134–155, https://doi.org/10.1016/j.jsames.2006.09.011.

Limarino, C.O., Césari, S.N., Net, L.I., Marenssi, S.A., Gutierrez, R.P. & Tripaldi, A. 2002. The Upper Carboniferous postglacial transgression in the Paganzo and Río Blanco basins (northwestern Argentina): facies and stratigraphic significance. *Journal of South American Earth Sciences*, **15**, 445–460, https://doi.org/10.1016/S0895-9811(02)00048-2.

Lucente, C.C. & Pini, G.A. 2003. Anatomy and emplacement mechanism of a large submarine slide within a Miocene foredeep in the northern Apennines, Italy: a field perspective. *American Journal of Science*, **303**, 565–602.

Macdonald, D.I.M., Moncrieff, A.C.M. & Butterworth, P.J. 1993. Giant slide deposits from a Mesozoic fore-arc basin, Alexander Island, Antarctica. *Geology*, **21**, 1047, https://doi.org/10.1130/0091-7613(1993)021<1047:GSDFAM>2.3.CO;2.

Masson, D.G., Huggett, Q.J. & Brunsden, D. 1993. The surface texture of the Saharan Debris Flow deposit and some speculations on submarine debris flow processes. *Sedimentology*, **40**, 583–598, https://doi.org/10.1111/j.1365-3091.1993.tb01351.x.

McGilvery, T.A. (Mac) & Cook, D.L. 2003. The Influence of Local Gradients on Accommodation Space and Linked Depositional Elements Across a Stepped Slope Profile, Offshore Brunei. *In*: *Shelf Margin Deltas and Linked Down Slope Petroleum Systems: 23rd Annual*. SOCIETY OF ECONOMIC PALEONTOLOGISTS AND MINERALOGISTS, 387–419., https://doi.org/10.5724/gcs.03.23.0387.

Milana, J.P., Kneller, B. & Dykstra, M. 2010. Mass-Transport Deposits and Turbidites, Syn-to-Post-Glacial Carboniferous Basins of Western Argentina. *ISC 2010 Field Guide*, 01–88.

Moscardelli, L., Wood, L. & Mann, P. 2006. Mass-transport complexes and associated processes in the offshore area of Trinidad and Venezuela. *AAPG Bulletin*, **90**, 1059–1088, https://doi.org/10.1306/02210605052.

Nissen, S.E., Haskell, N.L., Steiner, C.T. & Coterill, K.L. 1999. Debris flow outrunner blocks, glide tracks, and pressure ridges identified on the Nigerian continental slope using 3-D seismic coherency. *The Leading Edge*, **18**, 595–599, https://doi.org/10.1190/1.1438343.

Ogata, K., Mutti, E., Pini, G.A. & Tinterri, R. 2012. Mass transport-related stratal disruption within sedimentary mélanges: Examples from the northern Apennines (Italy) and south-central Pyrenees (Spain). *Tectonophysics*, **568**–**569**, 185–199, https://doi.org/10.1016/j.tecto.2011.08.021.

Ogata, K., Mountjoy, J.J., Pini, G.A., Festa, A. & Tinterri, R. 2014a. Shear zone liquefaction in mass transport deposit emplacement: A multi-scale integration of seismic reflection and outcrop data. *Marine Geology*, **356**, 50–64, https://doi.org/10.1016/j.margeo.2014.05.001.

Ogata, K., Pogačnik, Ž., Pini, G.A., Tunis, G., Festa, A., Camerlenghi, A. & Rebesco, M. 2014b. The carbonate mass transport deposits of the Paleogene Friuli Basin (Italy/Slovenia): Internal anatomy and inferred genetic processes. *Marine Geology*, **356**, 88–110, https://doi.org/10.1016/j.margeo.2014.06.014.

Omosanya, K.O. & Alves, T.M. 2013. A 3-dimensional seismic method to assess the provenance of Mass-Transport Deposits (MTDs) on salt-rich continental slopes (Espírito Santo Basin, SE Brazil). *Marine and Petroleum Geology*, **44**, 223–239, https://doi.org/10.1016/j.marpetgeo.2013.02.006.

Posamentier, H.W. & Kolla, V. 2003. Seismic Geomorphology and Stratigraphy of Depositional Elements in Deep-Water Settings. *Journal of Sedimentary Research*, **73**, 367–388, https://doi.org/10.1306/111302730367.

Posamentier, H.W. & Martinsen, O.J. 2011. The Character and Genesis of Submarine Mass-Transport Deposits: Insights from Outcrop and 3D Seismic Data. *In*: *Mass-Transport Deposits in Deepwater Settings*. SEPM (Society for Sedimentary Geology), 7–38., https://doi.org/10.2110/sepmsp.096.007.

Prior, D.B., Bornhold, B.D., Johns, M.W., Suhayda, J.N., Bornhold, B.D. & Johns, M.W. 1984. Depositional characteristcs of a submarine debris flow. *Journal of Geology*, **92**, 707–727, https://doi.org/00221376.

Puigdomenech Negre, C.G. 2014. *The Relationship between Deltaic and Turbidite Succession at Cerro Bola (LR - Argentina) and Vidal Ramos (SC - Brazil)*. Universidade do Vale do Rio dos Sinos.

Ramos, V.A. 1988. The tectonics of the Central Andes; 30° to 33° S latitude. *In*: *Special*

Paper of the Geological Society of America. Geological Society of America, Geological Society of America Special Papers, 31–54., https://doi.org/10.1130/SPE218-p31.

Sobiesiak, M.S., Kneller, B., Alsop, G.I. & Milana, J.P. 2016a. Inclusion of Substrate Blocks Within a Mass Transport Deposit: A Case Study from Cerro Bola, Argentina. *In*: Lamarche, G., Mountjoy, J., et al. (eds) *Submarine Mass Movements and Their Consequences, 7th International Symposium. Advance in Natural and Technological Hazards Research, Springer, The Netherlands.* Cham, Springer International Publishing, Advances in Natural and Technological Hazards Research, 487–496., https://doi.org/10.1007/978-3-319-20979-1_49.

Sobiesiak, M.S., Kneller, B., Alsop, G.I. & Milana, J.P. 2016b. Internal deformation and kinematic indicators within a tripartite mass transport deposit, NW Argentina. *Sedimentary Geology*, **344**, 364–381, https://doi.org/10.1016/j.sedgeo.2016.04.006.

Sobiesiak, M.S., Alsop, G.I., Kneller, B. & Milana, J.P. 2017. Sub-seismic scale folding and thrusting within an exposed mass transport deposit: A case study from NW Argentina. *Journal of Structural Geology*, **96**, 176–191, https://doi.org/10.1016/j.jsg.2017.01.006.

Valdez, V.B., Milana, J.P. & Kneller, B.C. 2015. Megadeslizamientos gravitacionales de la formación guandacol en Cerro Bola y Sierra de Maz y su relación con la glaciación del Paleozoico tardío, La Rioja, Argentina. *Latin American Journal of Sedimentology and Basin Analysis*, **22**, 109–133.

Valdez Buso, V. 2015. *The Geological Record of the Late Paleozoic Ice Age in Paganzo (Argentina) and Paraná (Brazil) Basins: Comparison of Sedimentary Successions and Glacial Cycles*. Unpublished PhD thesis, Universidade do Vale do Rio.

Zapata, T.R. & Allmendinger, R.W. 1996. Thrust-front zone of the Precordillera, Argentina: A thick-skinned triangle zone. *AAPG Bulletin*, **80**, 359–381, https://doi.org/10.1306/64ED87E6-1724-11D7-8645000102C1865D.

Figures

Figure 01: (a) Outline map of South America highlighting the late Palaeozoic sedimentary basins. Red rectangle locates the study area. Modified from Gulbranson *et al.* (2010); **(b)** Geological map of Cerro Bola (modified from Dykstra *et al.* (2011). Red arrow indicates the main transport direction (NW); **(c)** Stratigraphic column from Cerro Bola.

Figure 02: (a) Oblique photomosaic looking east towards Cerro Bola; **(b)** Line drawing showing the interpretation for the whole Cerro Bola stratigraphy. Note local contacts (erosive and/or pinching) between MTDs II and III and their respective substrate the Fluvio deltaic II and III. Location for figures 3, 4 and 5 are shown. The legend is the same as Fig. 01.

Figure 03: (a) Oblique aerial photograph looking southeast towards Cerro Bola; **(b)** General photograph showing MTD I with its green matrix and presence of sandstone and siltstone blocks embedded in MTD I; **(c)** Moderately deformed, bedded siltstone block with a drop-stone; **(d)** Deformational zone developed at the upper zone of the Fluvio-Deltaic I, commencing directly below MTD I. Note the highly deformed sediments in the deformation zone and the presence of small sandstone blocks within MTD I.

Figure 04: (a) Mosaic parallel to the inferred transport direction, showing MTD II stratigraphy and sandstone block distribution; **(b)** Photo showing the presence of co-genetic turbidites, followed by ponded turbidites deposited on top of the MTD. Note that the co-genetic turbidites thicken and thin as they drape the topographic lows and highs; **(c)** Photograph showing the deformation zone between MTD II and Fluvio-Deltaic II, where the zone is bounded at the top by MTD II and the base by a shear zone that separates deformed from undeformed sandstone; **(d)** Example of a large bedded sandstone block inside MTD II; **(e)** Example of original bedding preserved within a block, with cross stratification from the block at Fig. 04d.

Figure 05: **(a)** Aerial photo showing a section of MTD III and the indented undulating erosional surface between MTD III and Fluvio-Deltaic III. Note that the Fluvio-Deltaic is almost completely removed at the right-hand side of the image; **(b)** Close-up photo of the erosional surface and MTD III. Deformed and bedded strata within MTD III can be noticed as well as variably dipping bedded blocks; **(c)** Photomosaic of the northern part of Cerro Bola, displaying the internal divisions of MTD III. Lower zone shows coherently bedded sediments and above the disrupted strata from the upper zone; **(d)** Turbidite succession (ponded turbidite) that pinches out (towards the right hand side) and onlaps against the rugged topography of the MTD.

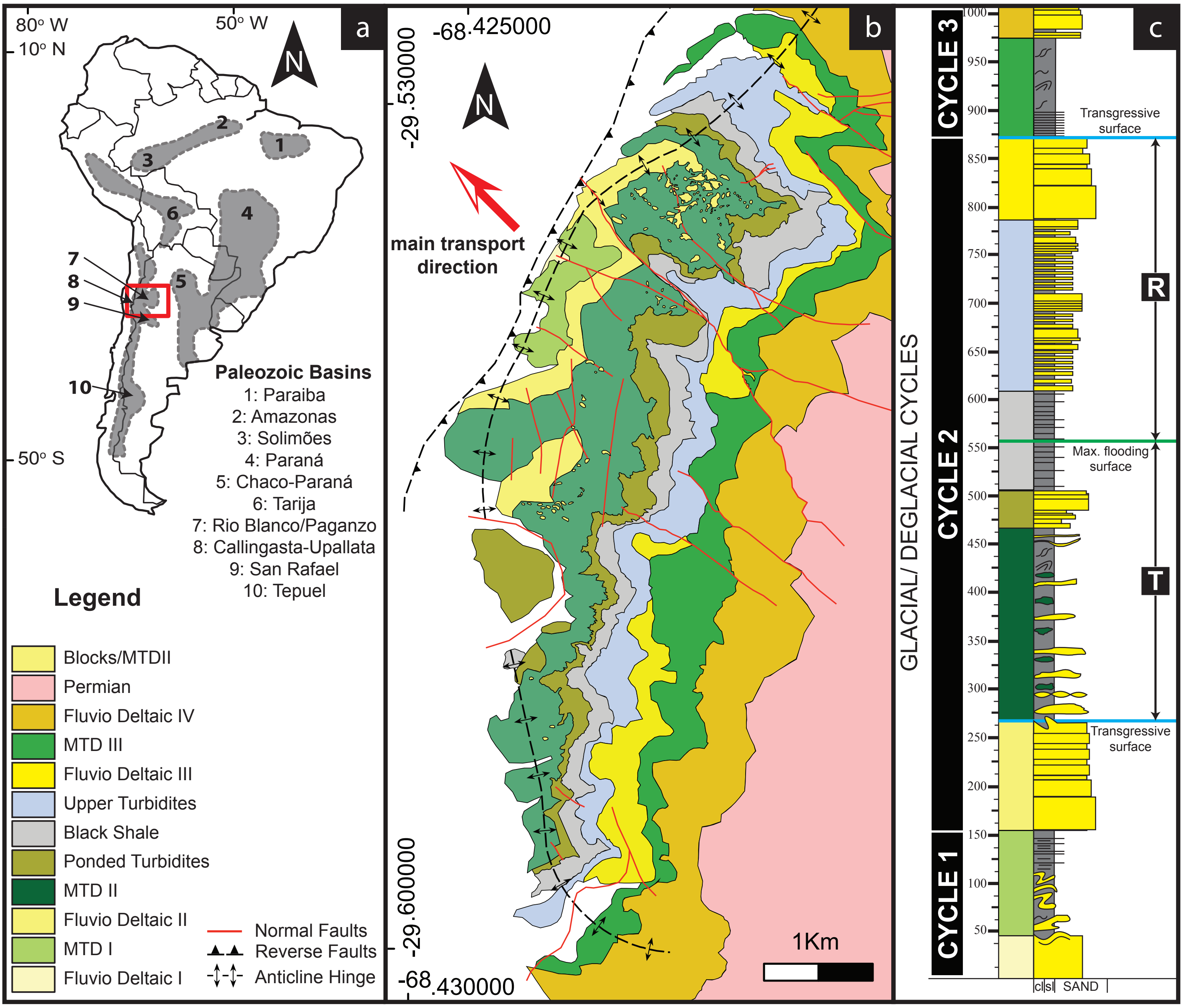
a
80° W
50° W
10° N
50° S
N
1
2
3
4
5
6
7
8
9
10
Paleozoic Basins
1: Paraiba
2: Amazonas
3: Solimões
4: Paraná
5: Chaco-Paraná
6: Tarija
7: Rio Blanco/Paganzo
8: Callingasta-Upallata
9: San Rafael
10: Tepuel
Legend
Blocks/MTDII
Permian
Fluvio Deltaic IV
MTD III
Fluvio Deltaic III
Upper Turbidites
Black Shale
Ponded Turbidites
MTD II
Fluvio Deltaic II
MTD I
Fluvio Deltaic I
Normal Faults
Reverse Faults
Anticline Hinge
b
-68.425000
-29.530000
-29.600000
-68.430000
N
main transport direction
1Km
c
GLACIAL/ DEGLACIAL CYCLES
CYCLE 1
CYCLE 2
CYCLE 3
1000
950
900
850
800
750
700
650
600
550
500
450
400
350
300
250
200
150
100
50
Transgressive surface
Max. flooding surface
Transgressive surface
R
T
cl sl SAND

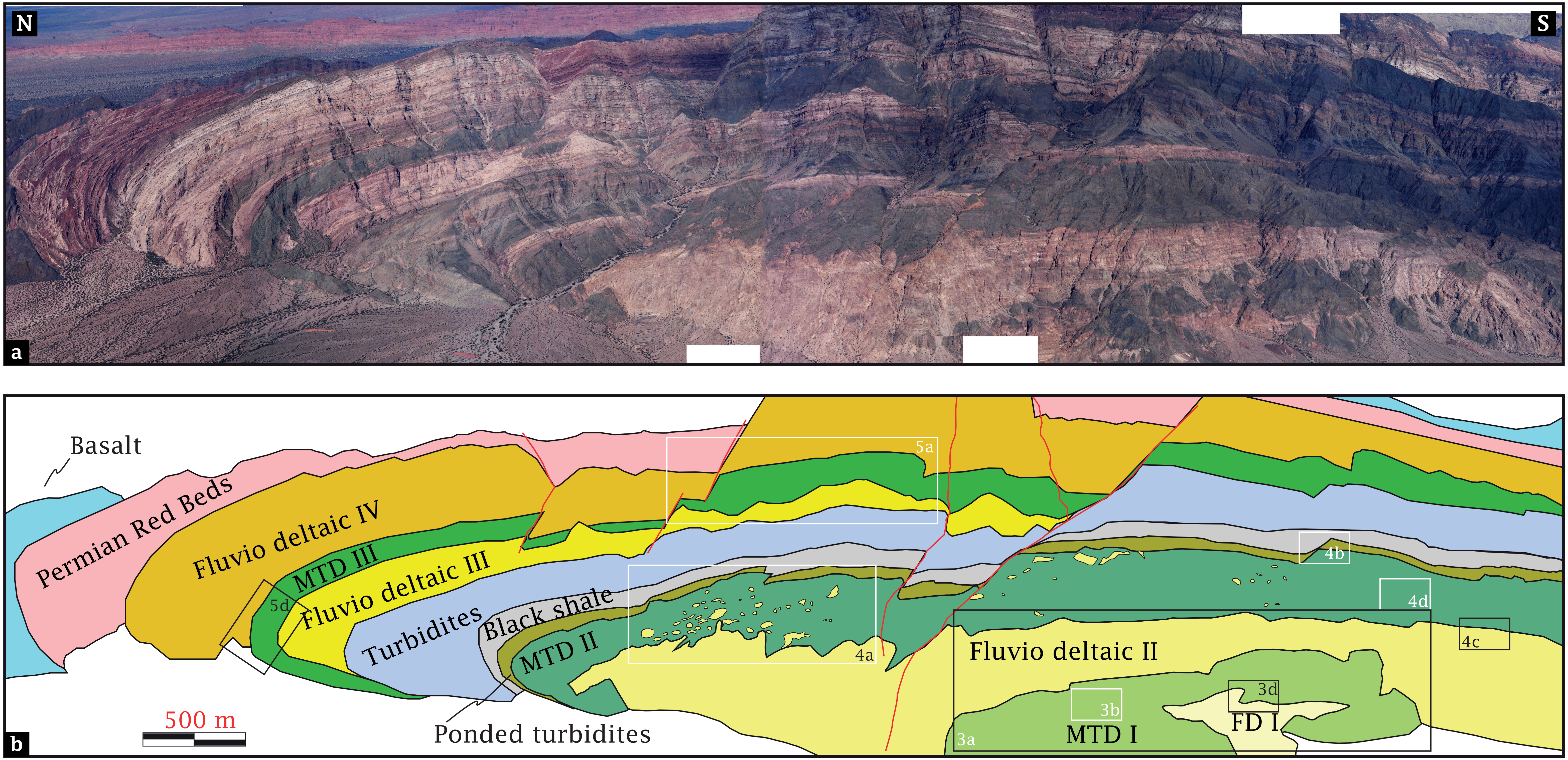
N
S
a
Basalt
Permian Red Beds
Fluvio deltaic IV
MTD III
Fluvio deltaic III
Turbidites
Black shale
MTD II
Ponded turbidites
Fluvio deltaic II
MTD I
FD I
5a
5d
4a
4b
4c
4d
3a
3b
3d
500 m
b

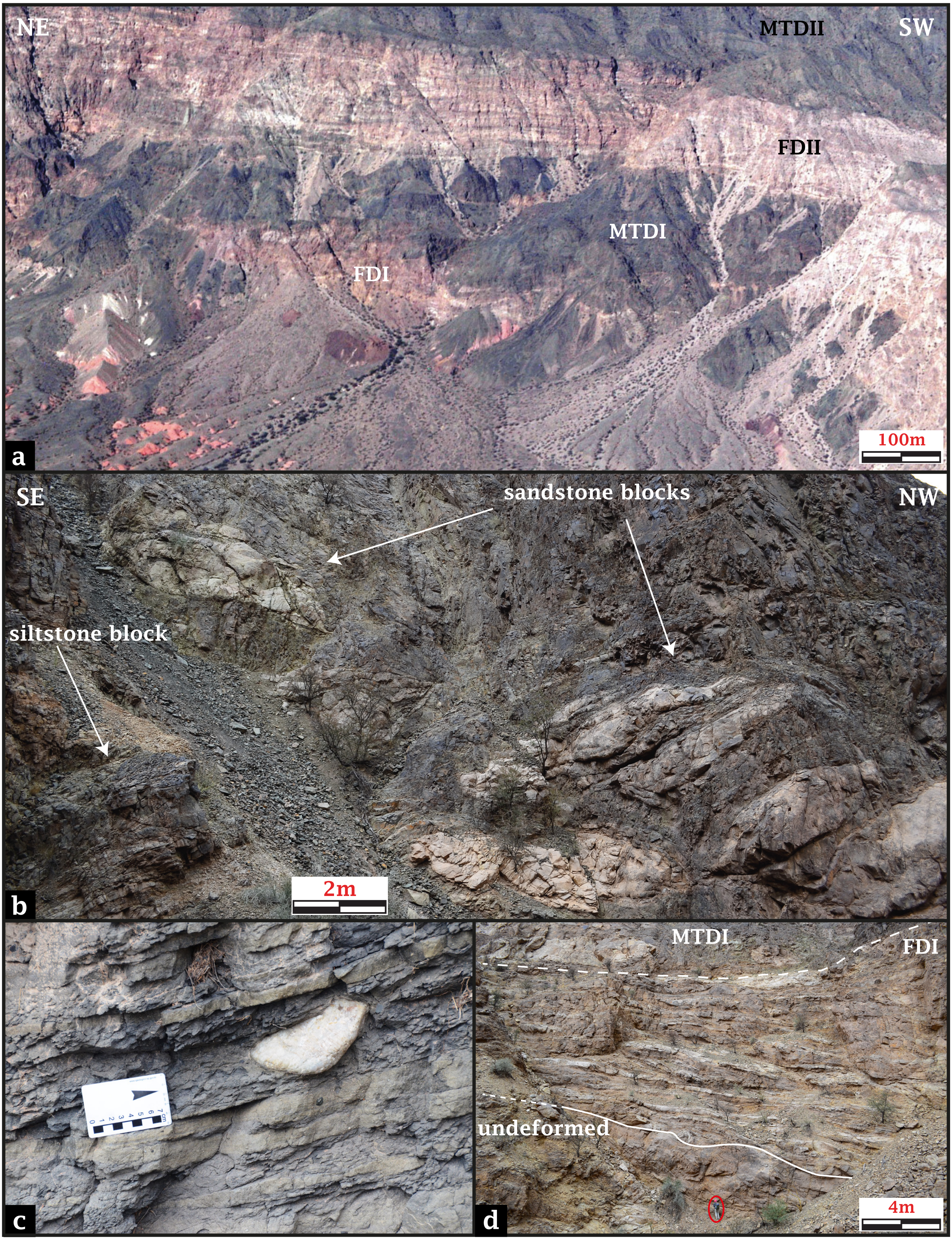
NE
MTDII
SW
FDII
MTDI
FDI
100m
a
SE
sandstone blocks
NW
siltstone block
2m
b
c
MTDI
FDI
undeformed
4m
d

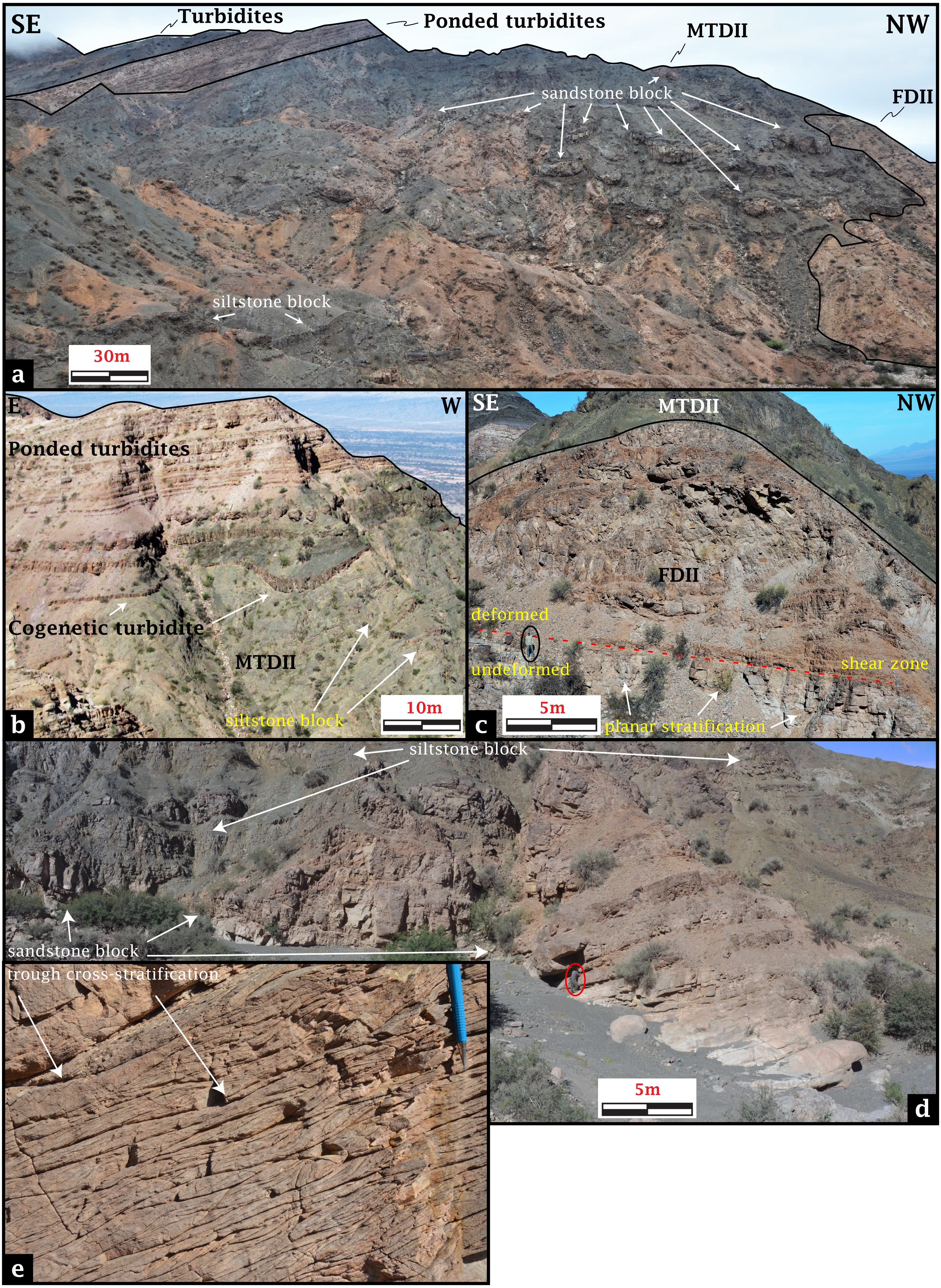
SE
Turbidites
Ponded turbidites
MTDII
NW
sandstone block
FDII
siltstone block
30m
a
E
W
Ponded turbidites
Cogenetic turbidite
MTDII
siltstone block
10m
b
SE
NW
MTDII
FDII
deformed
undeformed
shear zone
planar stratification
5m
c
siltstone block
sandstone block
trough cross-stratification
5m
d
e

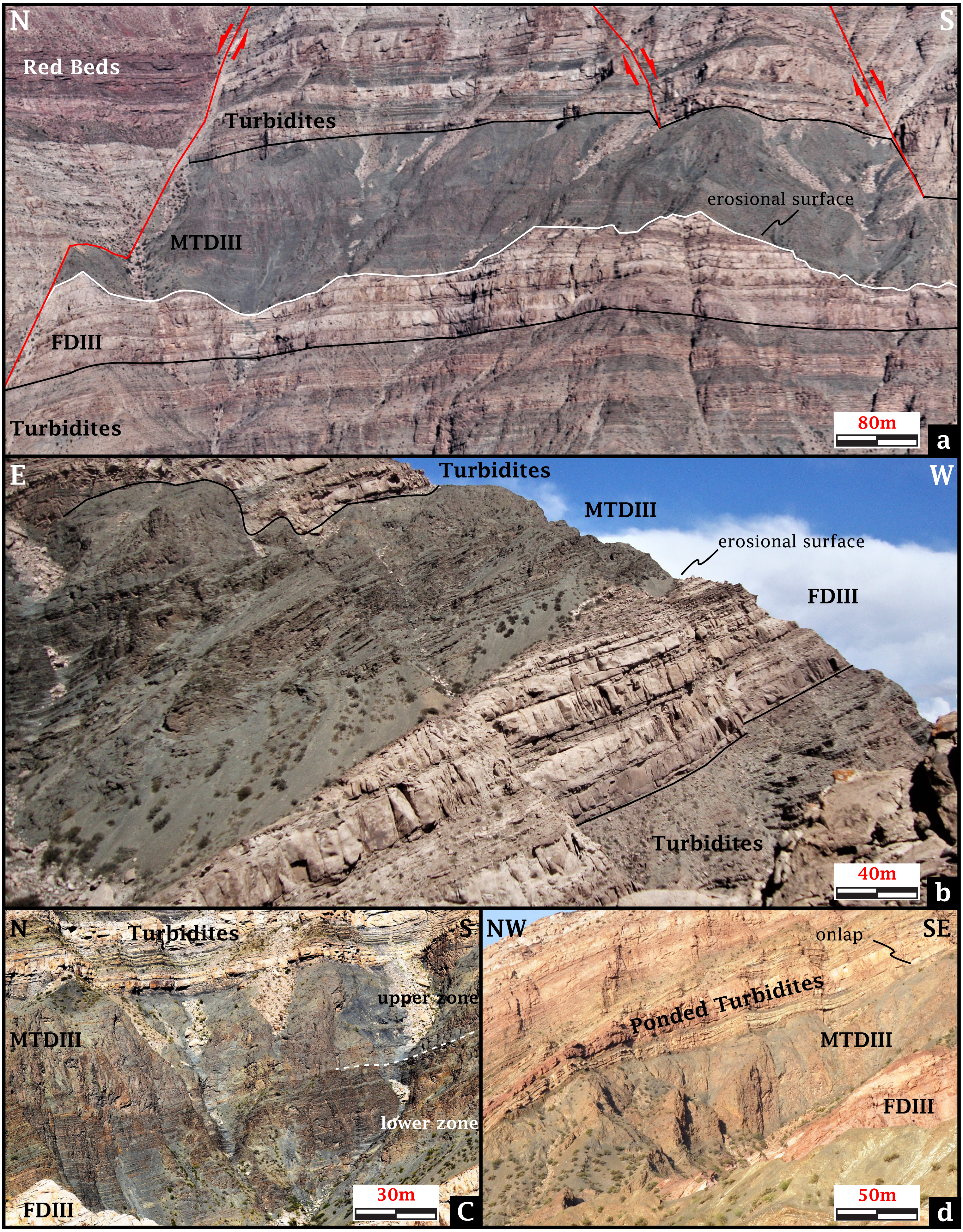
N
S
Red Beds
Turbidites
MTDIII
erosional surface
FDIII
Turbidites
80m
a
E
Turbidites
W
MTDIII
erosional surface
FDIII
Turbidites
40m
b
N
Turbidites
S
upper zone
MTDIII
lower zone
FDIII
30m
c
NW
onlap
SE
Ponded Turbidites
MTDIII
FDIII
50m
d